CONF-811026-14

FIFTH CONFERENCE

GEOPRESSURED - GEOTHERMAL ENERGY

U.S. GULF COAST

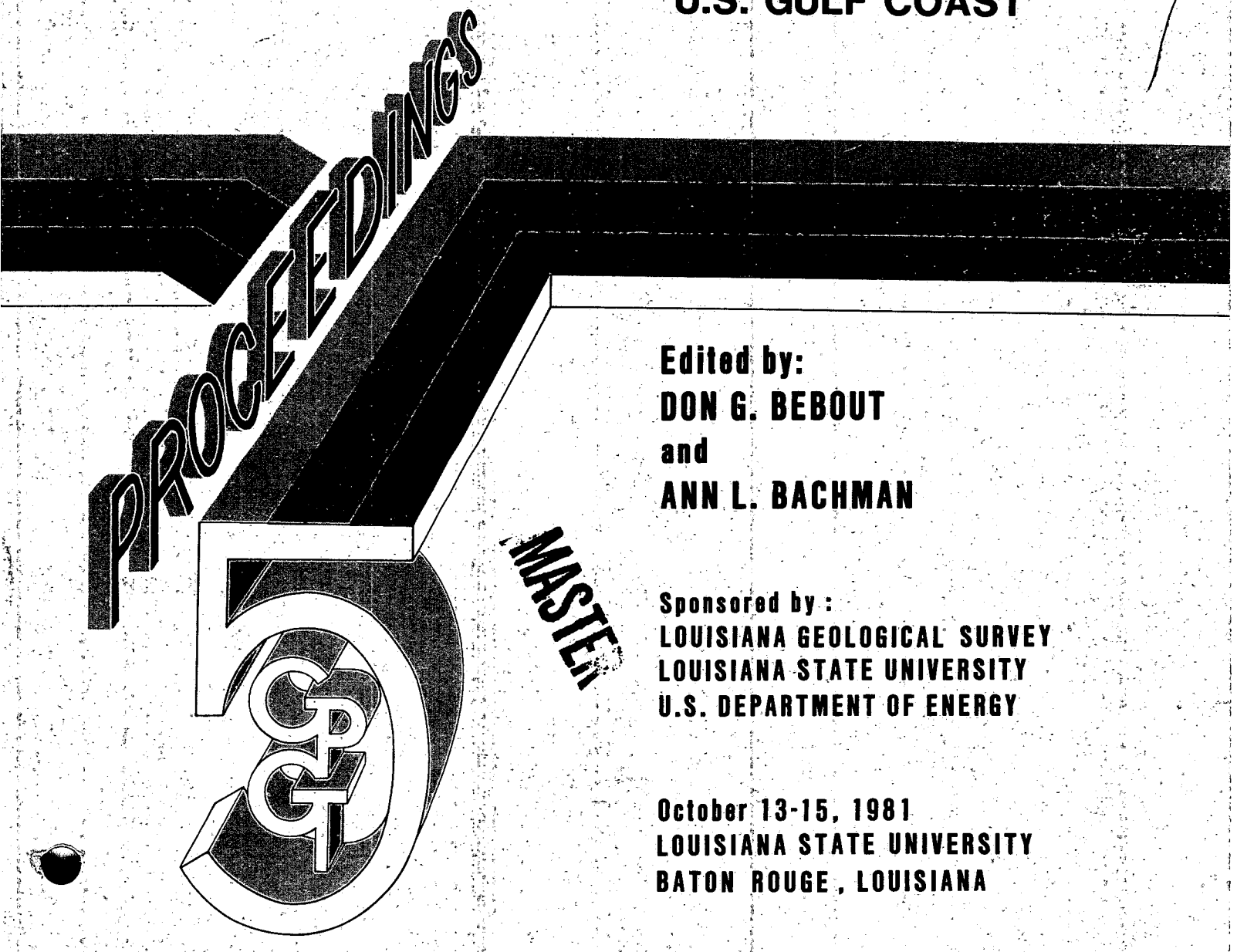

Edited by:
DON G. BEBOUT
and
ANN L. BACHMAN

Sponsored by :
LOUISIANA GEOLOGICAL SURVEY
LOUISIANA STATE UNIVERSITY
U.S. DEPARTMENT OF ENERGY

October 13-15, 1981
LOUISIANA STATE UNIVERSITY
BATON ROUGE, LOUISIANA

CONTRACT NO. DE-FG08-81NV10186

COMPACTION MEASUREMENTS ON CORES FROM THE PLEASANT BAYOU WELLS

P. N. Jogi, K. E. Gray, T. R. Ashman, T. W. Thompson

Center for Earth Sciences and Engineering, The University of Texas at Austin

ABSTRACT

Additional measurements of compressibility, compaction coefficients, porosities, permeabilities, and resistivities have been conducted on cores from Pleasant Bayou Wells #1 and #2. All rock parameters show non-linear behavior with changing reservoir or pore pressure, which is of interest in modelling reservoir performance and subsidence. Compressibilities and uniaxial compaction coefficients decline by a factor of 2 to 3 as reservoir pressure declines from geopressured to normal hydrostatic conditions. Porosity reductions are 6 - 8% while permeability reductions are on the order of 10 - 30% over that reservoir pressure range. Measured formation factors were 2 - 4 times log derived values for F. Matrix compressibilities were not insignificant relative to bulk compressibilities.

INTRODUCTION

In a previous paper, data on porosity, permeability, bulk compressibility, uniaxial compaction coefficient, and elastic moduli were presented for samples recovered from GCO-DOE Pleasant Bayou Wells #1 and #2.[1] Also data on relative permeability to brine at low methane saturations[2,3] and triaxial compression behavior[4,5] of geopressured-geothermal sandstone samples have been reported. In this paper, additional compaction data are presented for the Pleasant Bayou wells, including some resistivity data taken from a report in progress.[6]

THEORETICAL CONSIDERATIONS

Production of fluid from an underground reservoir results in changes in the reservoir and overburden that should be taken into account in modelling reservoir behavior and surface subsidence. Where lateral dimensions of the reservoir are large compared to its thickness, deformation is assumed to occur primarily in the vertical plane. Formation compaction due to pore pressure reduction is therefore expressed in terms of a uniaxial compaction coefficient, for which lateral deformation of the rock formations is taken to be zero. Commonly used stress-strain relations and expressions for the uniaxial compaction coefficient may be found in a previous paper.[1]

In addition to formation compaction with changing stress, other rock parameters such as porosity, permeability, and resistivity also change. Permeability may be determined, of course, with flow rate-pressure change measurements.

Static measurement of porosity changes can be obtained by:

1. Volumetric Strain & Expelled Water Volume Method

$$\phi = \frac{\phi_0 V_b - \Delta V_w}{V_b(1 - \Delta)} \quad (1)$$

where ϕ = porosity at any stress level
ϕ_0 = original porosity
V_b = bulk volume of sample

$\Delta = \varepsilon_a + 2\varepsilon_r$ = measured bulk volume change at each stress level
ΔV_w = expelled water volume

2. Measurement of Volumetric Strain Only:
If it is assumed that bulk volume changes are only due to pore volume changes i.e. $\Delta V_p \simeq \Delta V_b$[7], then

$$\phi = \frac{\phi_0 - \Delta}{1 - \Delta} \quad (2)$$

3. Expelled Water Volume Measurement:
Using the same logic and approximation as in (2) one obtains

$$\phi = \frac{\phi_0 V_b - \Delta V_w}{V_b - \Delta V_w} \quad (3)$$

Dynamic measurement of porosity with the time-average equation utilizes compressional wave velocities:[8]

$$\phi = \frac{V_L(V_m - V_f)}{V_f(V_m - V_L)} \quad (4)$$

where V_L = compressional wave velocity in pore fluid
V_M = compressional wave velocity in the rock matrix
V_f = compressional wave velocity in saturated rock

If R_0 is the resistivity of a rock sample fully saturated with fluid of resistivity, R_w, then the formation factor, F, of the sample is given by:[9]

$$F = \frac{R_0}{R_w} \quad (5)$$

and to a first approximation ,

$$F = \phi^{-m} \quad (6)$$

where m is called the cementation factor. For sandstones, the Humble formula,

$$F = .62\phi^{-2.15} \quad (7)$$

is often used.[10]

DISCLAIMER

EXPERIMENTAL APPARATUS AND PROCEDURE

The Simultaneous Property System (SPS) apparatus used in this work has been described in detail by Evans.[11] Simultaneous and independent control of overburden stress, confining pressure, and pore pressure allow measurements of static and dynamic moduli, porosity, permeability, and resistivity at various states of stress. Modifications for lateral permeability measurements on a cylindrical core are according to the work of Morita[12] and for resistivity measurements according to Tellinghuisen.[13] Compaction parameters obtained with the SPS have been reported earlier.[14,15,1]

Measured data consist of axial and radial stresses and strains; pore pressures; pore fluid displaced (or injected) during sample deformation; P and S wave velocities; voltage drop across the core for a given current flow; and pressure drop across the core for a given fluid flow rate. Tests were conducted on 2.75 inch diameter samples extracted from cores from GCO-DOE Pleasant Bayou Wells #1 and #2. The samples were saturated with 6% brine. Overburden pressure gradient was approximated at 1 psi/ft and pore pressure gradient from 1 psi/ft to 0.5 psi/ft to cover an effective stress range from initial, geopressured conditions to normally pressured conditions. The experimental procedure was as follows:

1. The jacketed sample was initially loaded by increasing axial stress(p_a), confining pressure, (p_c), and pore pressure (p_p), simultaneously in steps, up to a maximum pressure numerically equal to sample depth (in feet). Axial and radial strains were recorded at each pressure step as reference values for computational purposes.
2. Holding axial stress (overburden pressure) and radial strains as obtained in step (1) constant, the pore fluid pressure was decreased in steps to a value numerically equal to half the specimen depth. Constant radial strain in this step was maintained with the control of confining pressure. This condition was achieved with an on-line data acquisition computer. Radial strains were continuously monitored during this test as the pore pressure was decreased or increased. Confining pressure was adjusted to keep radial strain constant at the value obtained in step (1). The above steps were repeated while unloading the specimen.
3. Steps (1) and (2) were repeated in most cases using a maximum pressure corresponding to ½ psi/ft as well. Pore pressure in this case was varied from ½ specimen depth to atmospheric conditions. This was done in part to check the validity of the effective stress concept.

The following additional hydrostatic loading tests were also run on each sample to obtain information on bulk properties at both elevated and atmospheric pore pressure conditions:

4. The sample was loaded up to an overburden and pore pressure corresponding to sample depth. Keeping overburden pressure and confining pressure constant, pore pressure was decreased in steps up to ½ specimen depth and data recorded. The above steps were then repeated while unloading the sample.
5. The above hydrostatic test was repeated except that overburden pressure, confining pressure, and pore pressure were initially at half the sample depth.
6. After unloading, the sample was subjected to an increasing hydrostatic stress in steps up to a maximum of ½ specimen depth. The pore pressure was kept at atmospheric pressure in this test. The procedure was repeated while unloading the sample.
7. Finally, an unjacketed hydrostatic compression test was run on the sample by increasing the fluid pressure up to ½ specimen depth and then the sample was again unloaded.

Data in steps (1), (2), and (3) were used to compute C_m (dynamic and static) as well as modulii; data from steps (4), (5), and (6) were used to compute bulk compressibilities at elevated and atmospheric pore pressure conditions; step (7) was used to compute matrix compressibility. Porosity changes were calculated by methods given earlier. Permeability was computed in the above steps based on work by Morita.[12]

EXPERIMENTAL RESULTS

Figures 1 through 8 show typical plots of several parameters as functions of pressure and thus depict the general behavior of the rock samples tested.

As expected, stress-strain curves show considerable non-linearity under both hydrostatic (atmospheric and elevated pore pressures) and uniaxial compaction loading (Figs. 1, and 2, respectively). Unloading paths as usual do not retrace the loading paths and considerable non-symmetry is observed. This trend is observed in measured parameters as well during unloading and loading paths. Sample to sample variations occur and samples exhibit some permanent set on unloading in many cases.

Since samples were tested at two stress levels, the two sets of curves (as shown in most of the figures) in most cases when superimposed, were similar though slightly shifted in many cases While the effective stress concept is therefore applicable, it should be noted that the stress level at which a certain effective stress is achieved has some influence. Other factors probably involved in the shifting include matrix compressibilities that are not negligible, anisotropy, loading history, and permanent set.

Figures 3 - 6 show typical plots of C_m, ϕ, k and F under uniaxial compaction conditions as functions of stress at the two stress levels. Notice the non-symmetry of C_m for loading and unloading paths. Static values differ considerably from dynamic values.[1] This trend was visible in plots of elastic modulii as well. The difference between static and dynamic values is typical and expected since static values are measured at high stress levels with a low rate of loading, while dynamic values (though measured at high stress levels) involve small stress differences due to wave motion, propagated at a high rate of loading. In addition, dynamic data are less likely to be affected by microcracks than strains in static tests.

Figure 4 shows plots of porosity changes as

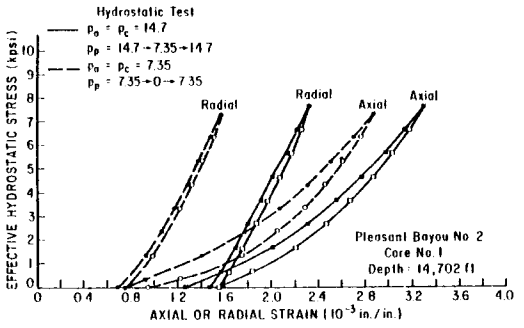

Fig. 1 Typical Stress-Strain Curves For Hydrostatic Loading

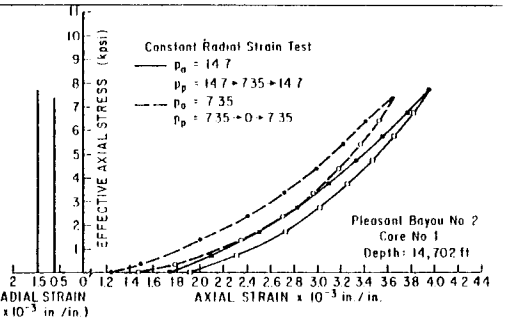

Fig. 2 Typical Stress-Strain Curves For Uniaxial Compaction.

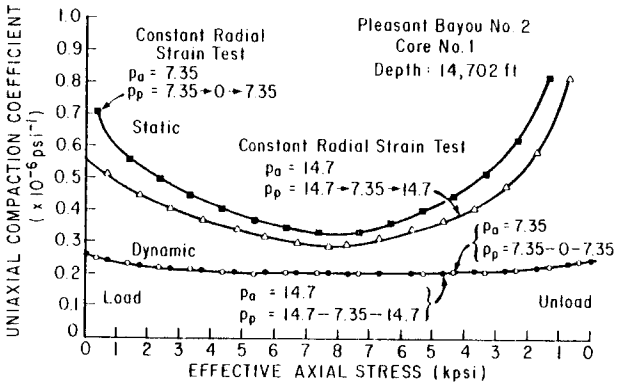

Fig. 3 Uniaxial Compaction Coefficients As Function of Axial Stress.

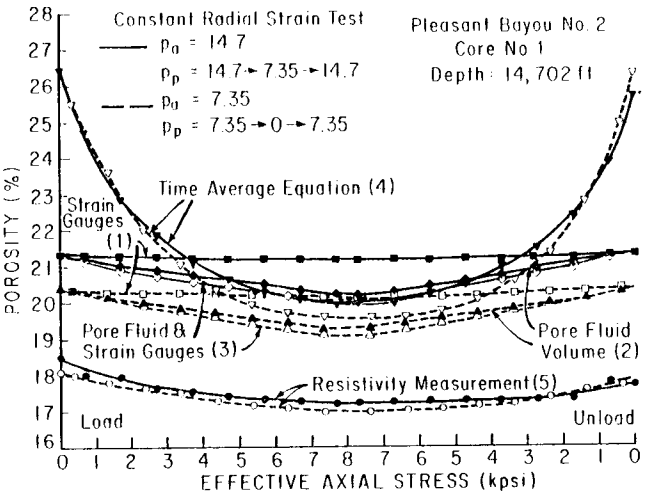

Fig. 4 Porosity As Function of Axial Stress.

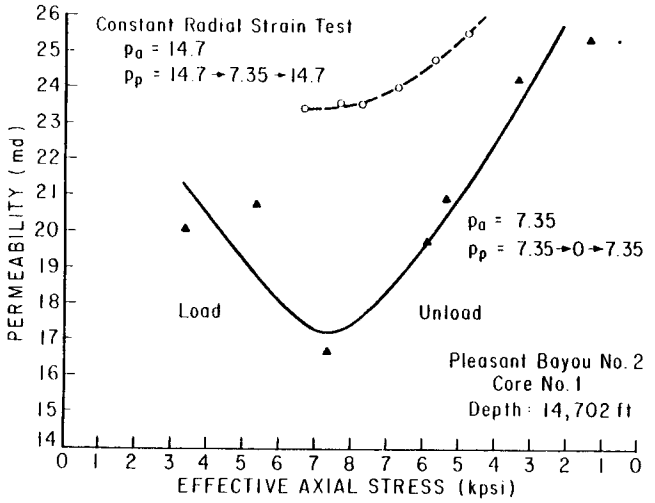

Fig. 5 Permeability to Brine as Function of Effective Stress.

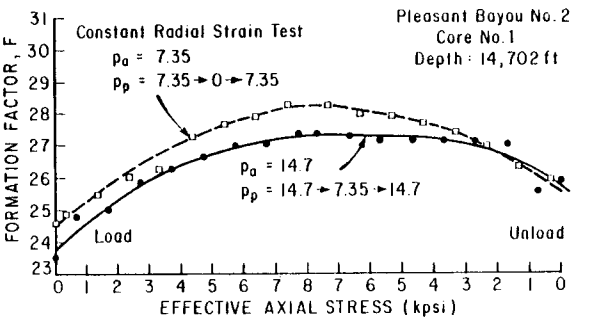

Fig. 6 Formation Factor As Function of Effective Stress.

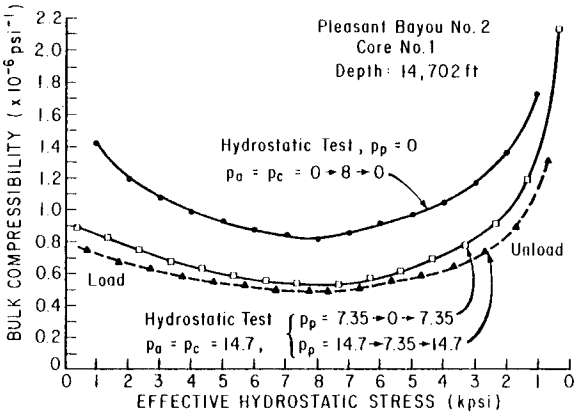

Fig. 7 Bulk Compressibility As Function of Hydrostatic Stress.

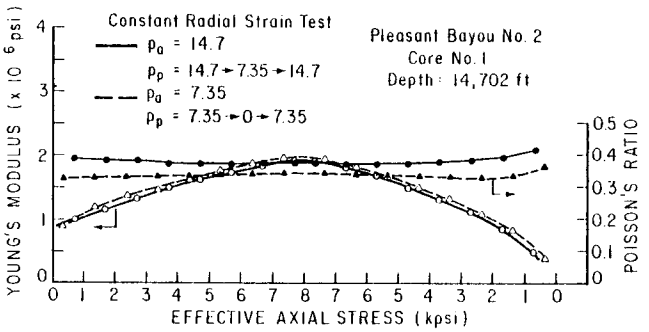

Fig. 8 Young's Modulus and Poisson's Ratio As Function of Axial Stress.

a result of changes in effective axial stress (overburden pressure-pore pressure). Resistivity porosity, curve (5) generally showed the same trend as the one using measured volumetric strain and expelled water volume method, curve 3. In many cases, curve 5 was shifted either slightly above or below curve 3. This discrepancy could be attributed to,(1) temperature effects; water resistivities, used for computing porosity changes, are more sensitive to small temperature changes than measured water volumes, and (2) direct use of the Humble formula as opposed to measured strains and expelled fluid method where initial porosity is used to compute the changes, and (3) some permanent set in the sample at the end of each test.

On comparing the statically measured porosities by various methods, porosity computed from measured strains gave the smallest percentage change in porosity for the effective stress change used in the experiments, while volumetric strain and expelled water volume method gave the largest change. This result could be due to the assumption of a negligible matrix compressibility compared to bulk compressibility on which measured strain or measured water volume expelled methods are based.[7]

However, pore volume changes given by curves 1, 2, 3, 5 do not agree with pore volume changes obtained by time average formula (curve 4). Based on curve 3, one observes that a small change in porosity occurs over a substantial effective stress change.

Figure 5 shows changes in permeability to brine as effective axial stress is increased or decreased during uniaxial compaction. Here also the two curves correspond to two stress levels at which the sample was tested as discussed earlier. Considerable scatter in data is observed. However, the trends in these tests are the same, and the effect of stress level is evident.

Figure 6 shows a typical plot of the variation of formation factor, F, with effective axial stress for the two stress levels. Observe that this curve like other plots is also non-linear and non-symmetrical. The stress dependence of F and its relationship with porosity is discussed in detail in a paper in publication.[6]

Figure 7 shows a typical plot of the variation of static bulk compressibility v/s hydrostatic stress. Three sets of curves shown in this figure correspond to values corresponding to zero pore pressure and elevated pore pressure conditions at two stress levels. The similarity of the three curves again demonstrates the applicability of effective stress concept for trend behavior, the compressibility value at a given value of effective stress, being a function, however, of the stress level involved. Notice the usual non-symmetry of the curves during loading and unloading.

Figure 8 shows Young's modulus and Poisson's ratio as a function of effective axial stress at the two stress levels tested. Neither parameter is very sensitive to stress level; Young's modulus varies with effective stress but Poisson's ratio does not.

Table I summarizes the results from several tests. An approximate range in the values of each parameter is given as the effective stress is increased from minimum to maximum value. Non-symmetry of loading and unloading paths is ignored here for summary purposes.

Some general observation may be summarized as follows:

1. Bulk compressibilities show a decrease of 55 -65% as effective axial stress is increased to its maximum value.

2. Bulk compressibilities at atmospheric pore pressure are higher than the values obtained at elevated pore pressures for the same level of effective stresses. This shows that matrix compressibilities are not insignificant as is often assumed.

3. Uniaxial compaction coefficients, C_m, range similarly as bulk compressibility values. At the same effective stress level, C_m is approximately ½ of bulk compressibility.

4. C_m values obtained over the same effective axial stress range (approximately 7500 psi) but at lower levels of overburden stress (7500 to 15000 psi) and pore pressure (0 to 7500 psi) were

TABLE 1

Reservoir Rock Parameters, GCO-DOE #1 & #2

	Stress* Level	Bulk Compressibility** ($x10^{-6}psi^{-1}$) p_c=constant p_p=varies	Bulk Compressibility** ($x10^{-6}psi^{-1}$) p_c=increasing p_p=0	Uniaxial Compaction Test** c_m ($x10^{-6}psi^{-1}$)	ϕ(%)	k(md)	F
GCO-DOE #1							
1-4-11755†	H	1.4 - .71	2.4 - .87	1.22 - .45	19.65 - 19.13	20.5 - 15.5	21.1 - 25.2
	L	2.0 - .84		1.17 - .43	19.31 - 18.94	11.5 - 11.0	23.9 - 27.52
1-7-14751	L	.78- .43		.64 - .21	19.31 - 18.99	86 - 70	23.0 - 25.31
14765	H			.40 - .23	17.63 - 17.34	69 - 62	16.99- 21.13
GCO-DOE #2							
2-1-14696	H			.60 - .21	18.23 - 17.89	92 - 83	26.25- 30.46
14696	H	1.0 - .48		.87 - .29	17.18 - 16.93	7.2 - 4.2	27.6 - 32.35
	L	1.1 - .50		.67 - .29	17.18 - 16.30	7.4 - 5.2	22.15- 27.76
14699	H	.88- .41	1.30- .71	.42 - .19	16.77 - 16.38	91 - 87	22.9 - 26.74
	L	1.1 - .44		.60 - .22	16.77 - 16.27	115 - 94	21.3 - 26.45
14702†	H	1.3 - .48	1.73- .81	.73 - .29	19.52 - 19.17	25.5 - 23.4	23.75- 27.40
	L	2.1 - .52		.90 - .32	19.47 - 19.06	25.5 - 17.2	24.6 - 28.25
14703	H	1.4 - .61		.84 - .31	16.95 - 16.77	26.8 - 19.5	24.10- 28.15
14711†	H	1.4 - .45	1.35 - .73	.52 - .23	21.16 - 20.90	168 -155	18.1 - 19.25
	L	1.6 - .56		.57 - .23	21.2 - 20.78	144 -121	16.7 - 18.5
14712	H		1.33 - .76	.84 - .29	19.16 - 19.02	26 - 19	23.3 - 25.80
	L	1.95- .52		.47 - .235	19.16 - 18.94	38.5 - 35	23.55- 25.80
2-3-15665†	L	1.1 - .53		.80 - .30	19.68 - 19.25	79 - 66.5	21.15- 23.63
15668	H	.83- .37	1.3 - .68	.48 - .19	19.82 - 19.58	69 - 51.5	25.5 - 29.25
	L	1.0 - .41		.99 - .29	19.75 - 19.27	68 - 56.5	26.3 - 30.2

* H - Corresponds to the initial stress condition on the specimen, $p_a=p_c=p_p$=specimen depth
L - Corresponds to the initial stress condition on the specimen, $p_a=p_c=p_p=\frac{1}{2}$ the specimen depth

† Measured matrix compressibilities varies from 0.31 to 0.33 x $10^{-6}psi^{-1}$.

** Range shown as effective stress increases from low to high values

significantly higher[1] than C_m values obtained at overburden stress of 15,000 psi and pore pressure varying from 15,000 - 7500 psi. This is due to the higher values of confining pressure required to keep lateral deformation zero at the higher stress levels involved in these tests.

5. Porosity reductions are lower than corresponding permeability reductions which suggests that preferential closure of flow channels/cracks takes place as a result of compaction.

6. Resistivity increase and consequently the increase in formation factor follows the same trend as porosity reductions.

7. The effective stress law applies well in terms of trends in rock parameters with pressure.

However, the numerical values for those parameters depend upon the stress levels involved in achieving a particular value of effective stress.

LAB DATA COMPARISON WITH LOG DATA

Values for porosity, uniaxial compaction coefficient, Young's modulus, Poisson's ratio and Formation factor as obtained from well logs in well #2 are compared with measured values for those parameters in Tables 2, 3, and 4.

Values of porosity were obtained from compensated sonic, neutron, density and induction logs and compared with lab determined dynamic and static values as well as values derived from measured re-

TABLE 2

Porosity (%)

	Laboratory Data						Log Derived Values			
	Resistivity		Static		Dynamic					
	Maximum Effective Stress	Minimum Effective Stress	Maximum Effective Stress	Minimum Effective Stress	Maximum Effective Stress	Minimum Effective Stress	Neutron	Density	Sonic	Resistivity
GCO-DOE #2										
2-1-14696 #1	16.2	17.3	17.89	18.23	15.85	21.5	17.85	15.6	16.02	34.3
#2	15.85	17.10	16.93	17.18	16.2	23.0				
14699	17.32	18.65	16.38	16.77	18.0	22.00	22.00	18.5	19.35	31.6
14702	17.20	18.10	19.17	19.52	19.85	26.0	19.20	13.65	18.07	27.6
14703	16.95	17.75	16.77	16.95	17.30	21.5	19.20	15.30	17.71	31.6
14711	21.95	22.50	20.90	21.16	19.80	24.5	18.90	16.5	17.45	37.1
14712	17.60	18.60	19.02	19.16	20.30	27.2	20.25	17.10	18.26	36.9
2-3-15665	18.4	19.30	19.25	19.68	21.25	23.5	12.45	16.80	16.79	24.0
15668	16.70	17.75	19.58	19.82	18.25	25.8	12.30	15.6	16.24	20.6

TABLE 3

Comparison of Log-Derived & Measured Uniaxial Compaction Coefficients & Formation Factors

	Uniaxial Compaction Coefficient ($x10^{-6}psi^{-1}$)						Formation Factor		
	Laboratory Data				Log Data		Laboratory Data		Log Derived Value
	Static		Dynamic						
	Maximum Effective Stress	Minimum Effective Stress	Maximum Effective Stress	Minimum Effective Stress	Sonic & Denisty Log	Mechanical Properties Log	Maximum Effective Stress	Minimum Effective Stress	
GCO-DOE #2									
2-1-14696	.285	.87	.17	.21	.168	.177	32.35	27.60	6.2
14699	.185	.42	.185	.212	.193	.195	26.75	22.9	12.0
14702	.285	.73	.20	.26	.179	.151	27.4	23.75	9.85
14703	.310	.84	.18	.22	.179	.155	28.15	24.1	7.38
14711	.230	.52	.20	.24	.183	.187	19.25	18.1	5.23
14712	.29	.84	.20	.26	.184	.187	25.8	23.3	5.29
2-3-15665	.30	.80	.21	.24	.175	.167	23.63	21.15	13.35
15668	.19	.48	.20	.25	.170	.176	29.25	25.5	18.5

sistivities. Uniaxial compaction coefficients were obtained from mechanical properties log as well as sonic and density logs using the following relations:[8]

$$\nu = \frac{3}{(\frac{2GC_b}{3} + 2)} - 1 \qquad (8)$$

$$C_m = \frac{1}{3}\frac{1+\nu}{1-\nu} C_b \qquad (9)$$

$$C_m = 2.24 \times 10^{-10} \times \frac{(\Delta t)^2}{3\rho_b} \qquad (10)$$

$$E = \frac{9G/C_b}{3/C_b + G} \qquad (11)$$

where C_b, G, ρ_b, Δt, which respectively represent bulk compressibility, shear modulus, density (bulk) and P wave travel time in the formation, were obtained from mechanical properties, density and sonic logs. From Tables 3 & 4, log derived values of uniaxial compaction coefficient, Young's modulus, and Poisson's ratio are substantially different compared to values obtained with pore fluid pressure decline. This means that the reservoir rock is relatively "stiffer" in wave propagation as compared to deformation resulting from pore pressure decline.

From Table 2, porosity values obtained from logs agree reasonably well with lab measurements, with the exception of values obtained from induction logs which gave high values. Dynamic values show the largest differences at low effective stresses. As mentioned earlier, porosity changes during deformation are not large.

The comparison of measured and log-derived formation factors (Table 3) shows significant differences.[16] Formation water resistivity determined from well logs is two to three times larger than values obtained from resistivity measurements in the lab. Thus, formation water salinity in the Pleasant Bayou geopressured well is higher than the logs would indicate. The amount of methane which can be dissolved in brine decreases with salinity, thus determination of correct water salinity is very important. Current work on using the S. P. log to predict water salinity is discussed in a paper by Dunlap and Dorfman.[17]

ACKNOWLEDGEMENTS

This work was sponsored by the Division of

TABLE 4

Comparison of Log Derived & Measured Values of Young's Modulus & Poisson's Ratio

	Young's Modulus ($x10^6psi$)			Poisson's Ratio		
	Lab Data (Static)			Lab Data (Static)		
	Maximum Effective Stress	Minimum Effective Stress	Log Derived Data	Maximum Effective Stress	Minimum Effective Stress	Log Derived Data
GCO-DOE #2						
2-1-14696	2.95	0.3	4.596	.355	.35	.277
14699	3.72	1.45	3.880	.321	.30	.293
14702	1.95	0.45	4.917	.372	.41	.307
14703	2.47	0.85	5.03	.291	.19	.300
14711	2.31	0.95	4.12	.281	.25	.287
14712	2.4	0.80	3.99	.321	.23	.287
2-3-15665	2.37	0.95	4.875	.312	.251	.250
15668	3.77	1.20	5.193	.331	.225	.230

Geothermal Energy, Department of Energy. That support is gratefully acknowledged, as well as the support of research personnel at the Center for Earth Sciences & Engineering. DOE Contract No. DE-AC08-79ET-27112.

REFERENCES

1. Gray, K. E., Jogi, P. N., Morita, N., & Thompson, T. W., "The Deformation Behavior of Rocks from the Pleasant Bayou Wells," Proc. Fourth U. S. Gulf Coast Geopressured-Geothermal Energy Conf., October 29-31, 1979, University of Texas at Austin, Vol. 2, pg. 1031.
2. Morita, N., Roberts, B. W., Gray, K. E., & Silberberg, I. H., "Relative Permeability Measurements of Rocks from the Texas Gulf Coast Geopressured-Geothermal Reservoirs at Low Free Gas Saturations," Trans. Geothermal Resources Council, September, 1980, Vol. 4, pg. 369.
3. Roberts, B. W., "Relative Permeability Measurements of Texas Gulf Coast Sandstones at Low Free Gas Saturations," M. S. Thesis, University of Texas at Austin, August, 1980.
4. Jogi, P. N., Llewellyn, B. C., and Gray, K. E., "Failure Studies on Texas Gulf Coast Geopressured-Geothermal Sandstones and Shales," to be presented at 1981 Annual Meeting, Geothermal Resources Council, October 25-29, 1981, Houston, Texas.
5. Llewellyn, B. C., "Compaction and Failure Studies on Texas Gulf Coast Geopressured Geothermal Sandstones & Shales," M. S. Thesis, University of Texas at Austin, May, 1980.
6. Ashman, T. R., "The Interrelationships and Variations of the Resistivity, Porosity, and Permeability as Functions of Pressure in a Geopressured Reservoir," M. S. Thesis, University of Texas at Austin, August, 1981.
7. Gertsma, J., "The Effect of Fluid Pressure Decline on Volumetric Changes in Porous Rocks," Petr. Trans., AIME, V 210, pp. 331-340, 1957.
8. Schlumberger, Limited, "Log Interpretation," Vol I, Principles, Schlumberger Ltd, New York, 1972.
9. Archie, G. E., "The Electrical Resistivity Log as an Aid in Determining Some Reservoir Characteristics," Trans., AIME, Vol 146, 1942, pg. 54.
10. Winsauer, W. O., Shearin, H. M., Jr., Masson, P. H., & William, M., "Resistivity of Brine-Saturated Sands in Relation to Pore Geometry," AAPG Bull. Vol 36, No. 2, Feb., 1952.
11. Evans, W. M., "A System of Combined Determination of Dynamic & Elastic Properties, Permeability, Porosity & Resistivity of Rocks," Ph.D. Dissertation, University of Texas at Austin, 1973.
12. Morita, N., "Three Dimensional Permeability Measurements," Ph.D. Dissertation, The University of Texas at Austin, 1974.
13. Tellinghuisen, C. M., "Simultaneous Determination of Permeability & Resistivity," M. S. Thesis, University of Texas at Austin, August, 1976.
14. Thompson, T. W., Menezes, J. J., & Gray, K. E., "Laboratory Measurements of the Uniaxial Compaction Coefficient," Proc. 3rd Geopressured-Geothermal Energy Conference, Lafayette, La., 1977.
15. Thompson, T. W., Kim, C. M. & Gray, K. E., "The Influence of Elevated Pore Pressure on the Mechanical and Flow Behavior of Berea Sandstone and Leuders Limestone," 20th U. S. Symposium on Rock Mechanics, University of Texas at Austin, June 4-6, 1979.
16. Jogi, P. N., Llewellyn, B., and Gray, K. E., "Comparison of Log-Derived and Lab Determined Rock Parameters for Gulf Coast Geopressured-Geothermal Reservoirs," in preparation.
17. Dunlap, H. F. and Dorfman, M. H., "Problems and Partial Solutions in Using the S. P. Log to Predict Water Salinity in Deep Hot Wells," Proc. Fifth U. S. Gulf Coast Geopressured-Geothermal Energy Conference, Louisiana State University, October 12-13, 1981.